Hydrodynamics of a dual-orifice needle-free jet injector

Yatish Rane[†], Jeremy Marston^{*}

Department of Chemical Engineering, Texas Tech University, Lubbock, TX 79409, USA

Abstract

In the recent literature, it has been shown that an enhanced, multi-faceted, balanced immune response can be generated using a combined intradermal (ID) and intramuscular (IM) delivery of vaccines, especially for novel DNA vaccines. Needle-based injection for the combined ID/IM delivery may require separate injections, which may prove to be time consuming, and impractical for mass immunizations. In contrast, a novel multi-orifice jet injector could be used to deliver drugs at multiple penetration depths simultaneously, which may provide advantages such as ease of operation, elimination of sharps, and short injection timeframe (O(10 ms)).

Here, we consider a dual-orifice geometry with both a wide orifice (200 μ m – 400 μ m) for IM drug delivery and a narrow orifice (100 μ m) for ID drug delivery. Using numerical simulations, we found that, at a fixed upstream pressure, jet velocities through wide and narrow orifices do not vary significantly for low-viscosity fluids ($\lesssim 4\%$). However, it was previously hypothesized that the jet power, $P_j = \frac{\pi}{8} \rho d_j^2 v_j^3$, is a more appropriate parameter to characterize tissue penetration depth. Thus, the jet power could vary by a factor of ~ 10 , yielding different depths for the two orifices. Using non-dimensional analysis via Euler (Eu) and Reynolds (Re) numbers, we characterize the role of orifice geometry and driving pressure, to generate geometry-specific correlations in the Eu-Re parameter space to estimate the jet velocity and pressure losses. We also elucidate the orifice size ratios that are best suited for fractional doses of $\sim 100 \, \mu$ L to intradermal tissue from a total injection of 1 ml.

Preliminary experiments to visualize the penetration of wide and narrow jet streams into gelatin and pork substrates showed that the wide jet stream leads to substantially greater penetration depth than the narrow jet stream. In summary, we provide the initial feasibility of simultaneous delivery of a drug to multiple penetration depths from the same injection cartridge using the needle-free jet injection technique.

[†]Present address: Intel Corporation, 2501 NE Century Blvd, Hillsboro, OR 97124, USA.

^{*}Corresponding author email: jeremy.marston@ttu.edu

1. Introduction

Delivery of vaccines or therapeutic drugs is most commonly achieved using a conventional hypodermic needle and syringe, which is considered an effective and reliable delivery method, but has many disadvantages. Particularly, needle-based injections are associated with: (i) painful administration, (ii) foreign object (besides the drug) penetration below the skin surface, and (iii) risk of needle-stick injuries¹, needles reuse² and secondary contamination. In needle-based injection, the selection of needle size should be based upon the target tissue^{3,4}. However, incorrect selection may result in incorrect penetration depth and, potentially, shoulder injury and bone-damage due to over-insertion of the needle^{5,8}. These issues associated with hypodermic needles can be tackled by several novel drug delivery technologies^{9,14}, which may include needle-free and pain-free drug delivery techniques. One such drug delivery technique is needle-free jet injection, which uses a high-speed liquid jet to deliver drugs across the skin and deposit inside the target tissue. Due to the simple mechanism and low manufacturing costs, spring-powered needle-free jet injection devices have an immense potential in mass immunizations¹⁵, especially in areas lacking infrastructure for dealing with bio-hazardous sharps waste.

Previous studies¹⁶⁻²⁰ have shown that needle-free jet delivery generates an enhanced immune response as compared to conventional needle-based delivery, especially for novel DNA vaccines. From the literature²⁰⁻²⁴, we can glean a brief overview of different types of immune responses using different drug delivery techniques. The immune system can be categorized into two parts²⁵, namely: 1) Innate immune system and 2) Adaptive immune system. The adaptive immune system can further be categorized into (i) humoral immunity, and (ii) cell-mediated/cellular immunity. These complex immune systems rely on a variety of different cells present in different tissues or body parts. For immunizations, it may be desirable for a vaccine to elicit a balanced multi-faceted immune response, which may dictate the vaccine dosage and target tissue for the vaccine. Most vaccines, including novel DNA vaccines, are currently administered through the intramuscular route^{26,27}. One of the advantages²¹ of an IM drug delivery is the ability of muscle tissue to retain a larger volume/dosage of drug as compared to the other tissues. IM tissue is also highly vascularized, with rich blood supply²⁸⁻³⁰, and thus providing greater ability for drug transport within the tissue. However, some previous studies^{24,31,32} have suggested that muscle has fewer antigen-presenting cells (APCs), which can reduce overall efficacy of vaccines. Other previous

works^{33,34} suggest that, in the absence of tissue damage or inflammation, muscle tissue contains relatively lower number of resident immune cells. Whereas the dermal tissues contains several APCs, including dendritic cells (in the dermis) and Langerhans cells (in the epidermis)²⁶, which help trigger the immune responses. However, since the ID tissue is typically 2-3 mm in depth, a more precise technique is required, and the volume delivered is lower than that for IM injection, with a typical fractional dose being 0.1 ml.

In electroporation (EP)-assisted drug delivery, one study³⁵ reported that IM delivery generated 10fold higher cellular immune response than ID delivery, whereas ID delivery generated higher antibody response (humoral immune response) than IM delivery. Therefore, several efforts^{21,23,31} have focused on combined ID/IM drug delivery to target the variety of immune cells present in both the tissue layers. These studies have consistently shown that combined ID/IM drug delivery enhance the overall immune response, especially for novel DNA vaccines. For EP-assisted drug delivery, previous research³⁶ reports a novel device for the combined ID/IM delivery, which was used for DNA vaccine delivery to elicit enhanced and balanced immune response as compared to either ID delivery or IM delivery alone. A needle-based combined ID/IM delivery may require multiple separate injections, which can be time consuming and impractical for mass immunizations. Here, we propose a combined ID/IM delivery using a needle-free jet injector, which may provide immense benefits such as ease of operation, short injection timeframe (O(10)ms)), and potentially enhanced immune response. In addition, such a system could potentially deliver multiple drugs at multiple penetration depths simultaneously. A needle-free jet injection targeted for IM delivery will first pass through the intradermal (ID) and subcutaneous (SC) tissues. However, it may not deposit any significant amount of the drug in each of those tissue layers. To gain the advantages of combined ID/IM drug delivery, we seek to deposit a sufficient amount of drug in each of those tissue layers (0.5 ml - 1 ml for IM drug delivery and \sim 0.1 ml for ID drug delivery), as reported by the literature^{21,23,31}, which we propose could be achieved using two separate jet streams, as sketched in figure 1.

To our knowledge multi-orifice devices have only been described sparingly in patents. For example, Daellenbach (2003) describes a multi-orifice adapter for the original Biojector® 2000 device to create broad liquid dispersion adjacent to internal organs³⁷. Crank (2015) also presents a similar multi-orifice design for injection via tubular devices such as endoscopes³⁸. Gilbert (2007)

details a device with multiple nozzles primarily for the purpose of intranasal delivery³⁹. In contrast, Hunter et al. (2010) specifically describes a transdermal multi-orifice jet injector with orifices set around the circumference of the nozzle for improved tissue dispersion⁴⁰. One very recent publication by McKeage et al. (2023)⁴¹ does report on a combined experimental-numerical investigation of a multi-orifice injector with capability of injecting through 7 orifices simultaneously, which shows excellent promise for large-volume subcutaneous delivery.

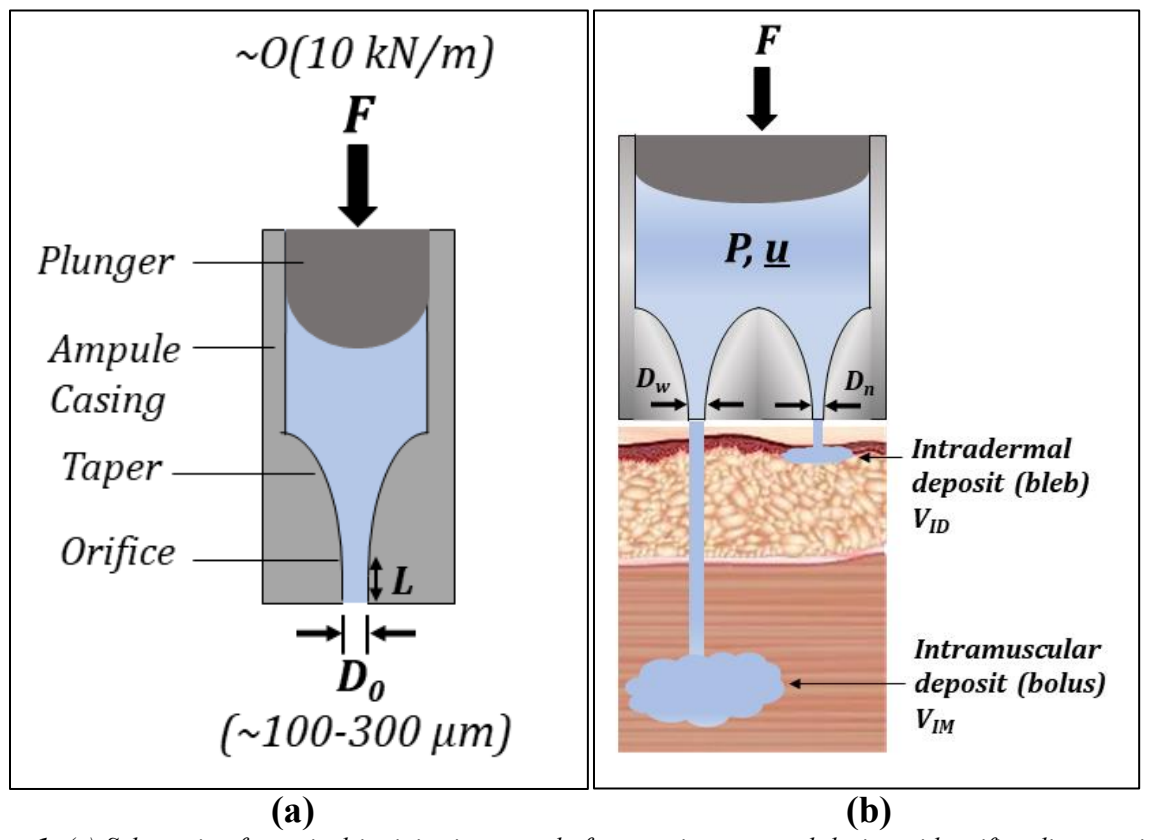


Figure 1. (a) Schematic of a typical jet injection ampule for a spring-powered device with orifice diameter in the range 100-300 μ m. (b) Schematic of a dual-orifice jet injector to achieve simultaneous drug delivery to both intramuscular tissue via a wide orifice (D_w) and intradermal tissue via a narrow orifice (D_v)

As such, the primary goal of this manuscript is to use numerical simulations to study the role of cartridge/orifice geometry on the hydrodynamics of dual-orifice jet injections, simultaneously targeting ID/IM delivery from a single ampule, and discuss the feasibility of practical implementation, via a limited experimental study.

2. Methods

2.1. Experimental setup

To guide simulations, we performed a limited set of experiments with a Bioject[®] ZetajetTM (see figure 2), a spring-powered device intended to deliver volumes up to 0.5 ml into either SC or IM tissue. As per the original manufacturer literature, the tissue depth with this device was dictated by selection of cartridge orifice size: "#2" and "#3" with orifice diameters of 0.004-inch (~102 μ m) and 0.006-inch (~152 μ m), respectively, were intended to target SC tissues (lateral triceps, abdomen, anterior thigh), whilst the "#4" with an orifice diameter of 0.008-inch (~203 μ m) was intended for IM tissues (deltoid). Here, to create a dual-orifice cartridge, we took the #2 cartridge and used microscopic drill bits to bore a hole (wider orifice) into the outer geometry of the Zetajet cartridge (as shown in figure 2). We thus consider the original Zetajet orifice to be the 'narrow orifice' (actual $D_n \approx 113 \ \mu$ m) and the drilled orifice to be the 'wide orifice' ($D_w \approx 300 \ \mu$ m or $D_w \approx 400 \ \mu$ m).

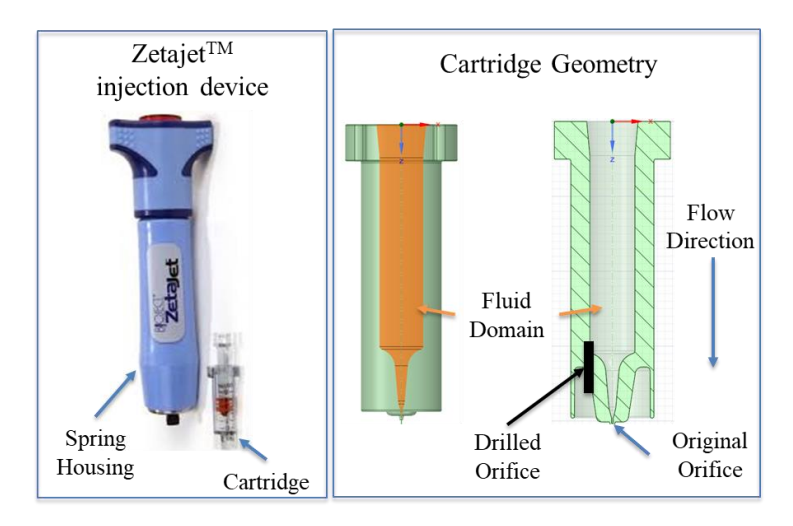


Figure 2. Left: ZetajetTM injection device and cartridge geometry. Right: Modification to the existing cartridge geometry to test the feasibility of a dual-orifice jet injector.

To visualize the simultaneous penetration of two liquid jets at two different depths, we use dyed DI water (1 mg/ml Trypan Blue from Sigma Aldrich) as a fluid (injectant) and gelatin hydrogel as the substrate (injectate). High-speed videography (Phantom V1611) is performed at 30,000 fps to capture the fluid distribution in gelatin hydrogel. Backlighting was achieved with the use of a LED array light source set 20-30 cm away from the subject to minimize heating, and a diffuser screen to achieve uniform background. To make the gelatin hydrogel, gelatin powder (gelatin from bovine

skin ~225 g bloom type B, Sigma Aldrich) (5% $_{\text{w/w}}$) is mixed with DI water at ~70 0 C and then the homogenized mixture is kept in a refrigerator (~ 10 0 C) for 24 hours to solidify. In addition, we visualize the fluid distribution of dyed DI water into pork muscle tissue (procured from local butcher), delivered using the multi-orifice jet injector.

2.2. Numerical simulations setup

In numerical simulations, we use computational fluid dynamics (CFD) software (Ansys Fluent v18.2) to design a variety of different cartridge/orifice geometries, meshing, and solving the fundamental governing equations over the fluid domain. The fundamental governing equations are the Navier-Stokes equations (for momentum balance) and the continuity equation (for material/mass balance), which are solved assuming state-state using SIMPLE (Semi-Implicit Method for Pressure Linked Equations) and RNG k-E turbulence model (for high Reynolds number $\left(Re_j = \frac{\rho v_j d_j}{\mu}\right)$ flow, where v_j = jet velocity, d_j = jet/orifice diameter, ρ = fluid density, μ = fluid viscosity). The assumption of steady flow was validated in our previous study⁴², for the main jet delivery, i.e., after the impulsive (piston slamming) phase, which typically lasts 2-3 ms. A single (liquid) phase, isothermal, incompressible flow system was assumed with negligible effect of gravitational forces. Here, we considered only water ($\rho = 998.2 \text{ kg/m}^3$, $\mu = 0.001 \text{ Pa.s}$) to mimic low-viscosity drugs such as insulin. In practice, it is not anticipated that fluid viscosities for injection would exceed O(0.1) Pa.s, thus low-viscosity fluids are the most applicable. To increase computational efficiency, we perform 3D symmetric simulation for the half cartridge geometry as shown in figure 3. A gradient meshing is employed with (quadratic element order) mesh density of ~11 nodes/mm in the upstream cartridge region and ~ 210 nodes/mm in the downstream orifice region (as per figure 3). The mesh density was guided, as with previous studies⁴², by the requirement that the error residuals for all velocity components and continuity equation were at most 10⁻⁶. In our previous studies^{42,43}, we performed experimental validation of numerical simulations for the steady-state flow at this level of accuracy, so that we can be confident of the choice of mesh.

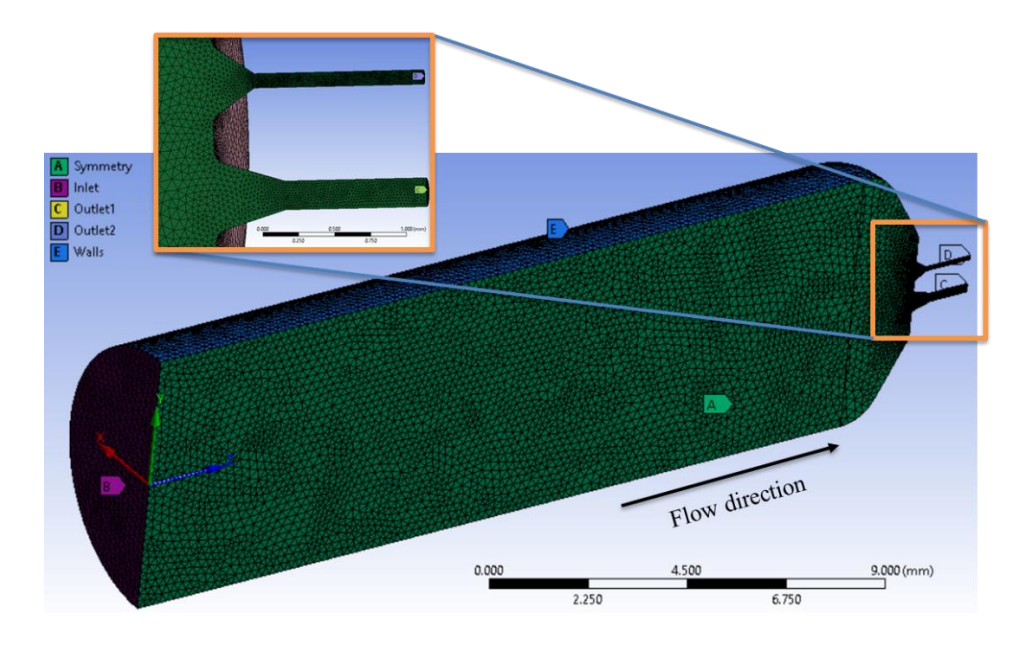


Figure 3. Numerical Simulations – an example for meshing setup for double-orifice jet injector in Ansys Meshing Software v18.2, with gradually increasing mesh density towards the orifices downstream.

Two important parameters that partially dictate the jet penetration depth are: 1) Jet/orifice diameter (d_j) and 2) Jet velocity (v_j) , which have either individually or collectively (via jet kinetic energy or jet power) been used to estimate tissue penetration depth⁴⁴⁻⁴⁸. In particular, the jet power is defined as follows:

$$P_{j} = \frac{\pi}{8} \rho d_{j}^{2} v_{j}^{3} \tag{1}$$

In line with recent reviews on penetration depths for various jet injectors (e.g., Mohizin & Kim⁴⁹; Schoppink & Fernandez-Rivas⁵⁰), the general consensus is that ID injections may require $d_j \sim 100$ – 150 microns and $v_j \sim 100$ – 150 m/s, whereas IM injections may require $d_j \sim 200$ – 400 microns and $v_j \sim 200$ – 300 m/s, and SC injections can be achieved using parameter values in between these two cases. In practice, these values may also depend on properties of the target tissue, such as skin tension, hydration at the time of injection, subcutaneous thickness, which are difficult to control. As such, in attempt to provide the simplest approach, we use the aforementioned parameter values (orifice diameters, velocity, etc.) established by literature⁴⁴⁻⁵³, as well as orifice lengths and driving pressures to guide our study. For simulations of dual-orifice jet injection, we thus choose to fix the narrow orifice ($d_n = 100 \, \mu m$) for ID injections and vary the wider orifice ($d_w = 200 \, \mu m$, 300 μm , 400 μm) for IM injections. For a particular double-orifice cartridge geometry, the orifice length to orifice diameter ratio was kept the same for both wide and narrow orifices ($L/d = L_n/d_n = L_w/d_w$),

and are guided by our previous works^{42,43}, where we used two distinct orifice length to orifice diameter ratios (L/d = 1.25 & L/d = 2.5). The distance between the orifices was set so that the openings were equidistant from the inner cartridge walls and from each other.

For needle-free jet injectors, the force from the actuation source (e.g., compressed spring) is used to pressurize the injection chamber (upstream cartridge region), which accelerates the fluid through the orifice (downstream cartridge region) to produce a liquid jet. Thus, to gain practical insights from our numerical simulation methodology, we implement a 'pressure-inlet' boundary condition, and outlet boundary condition to reflect outflow into the atmospheric pressure. Previous literature $^{51,54-58}$ was used to identify the experimental driving pressures used for a range of devices, which are typically between 10-20 MPa, based upon requirements for low-viscosity fluids to puncture skin and maintain high-speed jet flow. As such we set the inlet/upstream pressure values in the simulations to $(P_{inlet})_{water} = 10/15/20/25$ MPa. We further highlight a recent work by Williams et al 59 which explored the effect of viscous heat generation due to the high shear region at the walls in the orifice region of the cartridge; such effects were not considered in the simulations of the dual-orifices presented herein due to the low-viscosity where such effects are negligible, and hence our simulations are isothermal, but we refer the reader to section 3.3 for a detailed discussion of these effects in the context of viscous flow.

To characterize the effect of fluid viscosity and orifice geometries we employ dimensionless quantities – namely – Euler number (Eu) and Reynolds number (Re) for each orifice:

$$(Eu)_n = \frac{\Delta P}{\frac{1}{2}\rho(v_j)_n^2} \qquad , \qquad (Eu)_w = \frac{\Delta P}{\frac{1}{2}\rho(v_j)_w^2} \tag{2a}$$

$$(Re)_n = \frac{\rho(v_j)_n d_n}{\mu}$$
 , $(Re)_w = \frac{\rho(v_j)_w d_w}{\mu}$ (2b)

Where Eu, Re, d, v_j are the Euler number, Reynolds number, orifice diameter, and jet velocity, and the subscripts n and w represent the narrow and wide orifices, respectively. The pressure drop, used in the Euler number, across both orifices is given by $(\Delta P = (P_{inlet})_{gauge})$.

3. Results and Discussions

3.1. Numerical simulations for a dual-orifice jet injector

We begin our analyses with a qualitative overview of the flow of water in a dual-orifice injector, as shown in figure 4, for an upstream driving pressure of 25 MPa, with orifice diameter ratio of 1:3 ($d_n = 100$ and $d_w = 300$ µm). The pressure contour and velocity vectors are representative of the system at steady-state and indicate a uniform pressure field throughout the main cartridge body; Specifically, in figure 4(a), we see that majority (> 95%) of pressure losses occurs in the straight orifice region, after the conical taper. Therefore, it is essential to investigate the effect of orifice geometry on the pressure losses and the jet velocities through wide and narrow orifices.

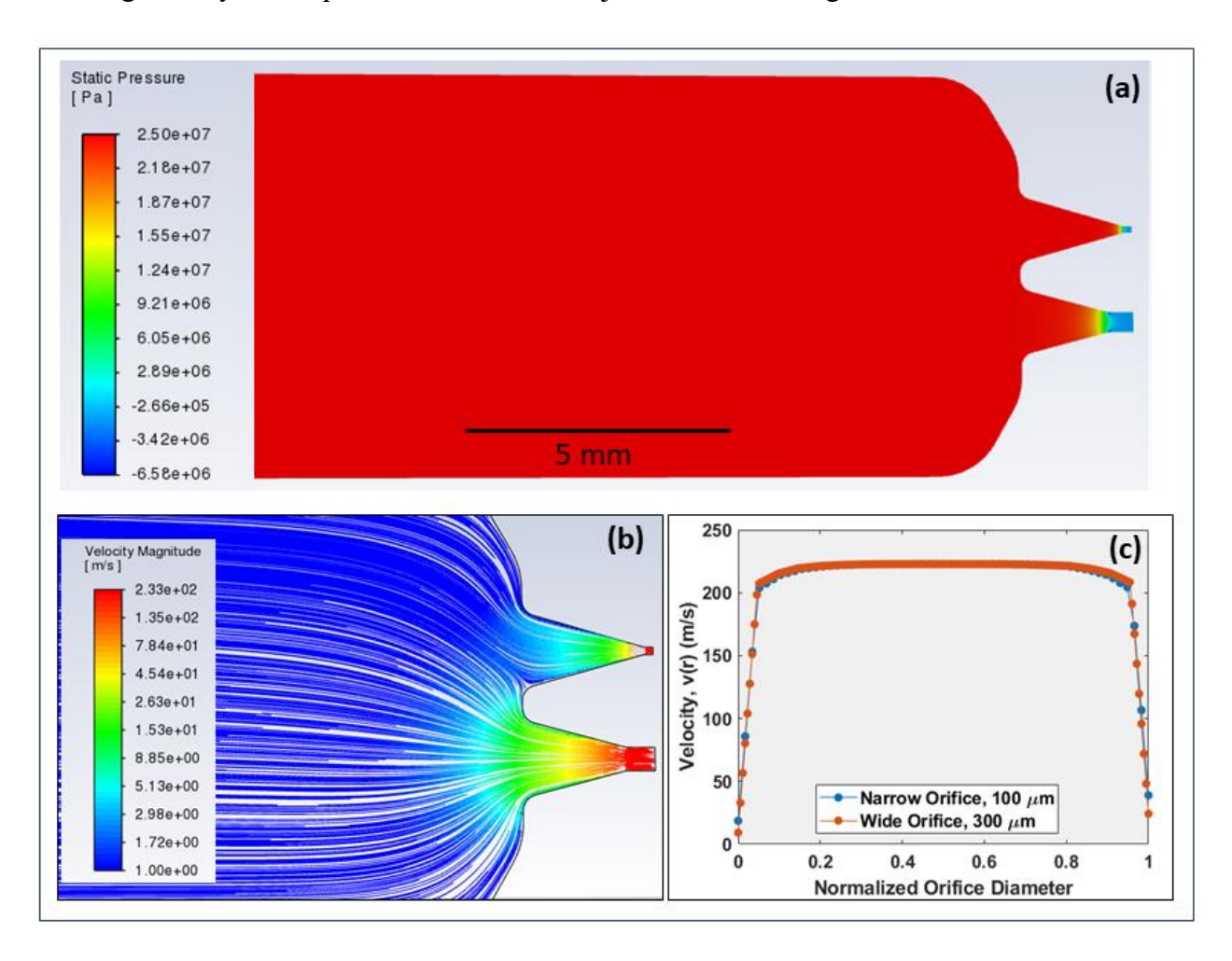


Figure 4. (a) Pressure contour and velocity vectors in a dual-orifice jet injection cartridge with water at driving pressure of 25 MPa. Wide orifice diameter – 300 μ m, Narrow orifice diameter – 100 μ m. L/d = 1.25 for both the orifices. (b) Zoomed view of the orifice region showing streamlines and velocity magnitude; (c) Outlet velocity profiles for wide and narrow orifices ($Re_n = 2.07 \times 10^4$, $Eu_n = 1.16$; $Re_w = 6.21 \times 10^4$, $Eu_w = 1.16$).

Assessing the jet speeds, we find $v_{max} = 222.8$ m/s for both orifices. Although the velocity profiles are clearly turbulent, they not fully developed due to the short orifice length and, as such, we estimate the average velocity as $v_{avg} = 0.95v_{max} = 211.7$ m/s and thus calculate the jet powers of each orifice as $P_n = 37.2$ W and $P_w = 334.5$ W. Using the data of Schramm-Baxter & Mitragotri⁴³ as the reference, these would lead to penetration depths of approximately 3-4 mm and 8 mm, respectively. Furthermore, these jet speeds yield flow rates (based on average flow speed) of $Q_n = 1.66 \times 10^{-6}$ m³/s and $Q_w = 1.49 \times 10^{-5}$ m³/s (i.e., 1.66 and 14.9 ml/s, respectively). As such, the total flow rate through both orifices would be 16.6 ml/s, and the total time for a 1 ml injection would be 60.2 ms.

Given the assumed penetration depths and individual flow rates above, this dual-orifice flow would thus deliver a fractional dose of 100 μ L to the ID tissue, and 900 μ L to the IM tissue. From a practical perspective, the typical fractional dose delivered to the ID tissue is on the order of 100 μ L, although there is some evidence⁶⁰ to show that a reduced volume closer to 50 μ L may be preferable from the perspective of increasing percentage delivery. Furthermore, IM doses are typically 0.5-1 ml, therefore this dosage split (ID:IM \approx 1:9) for either a total volume of 0.5 ml or 1 ml would render a split dose injection within the typical dosage ranges.

To observe the trends across a range of driving pressures and orifice diameter ratios, we now present the data for jet velocities and corresponding jet powers in figures 5(a)-(d), for L/d =1.25 and 2.5, and $d_w = 200$ and 300, respectively.

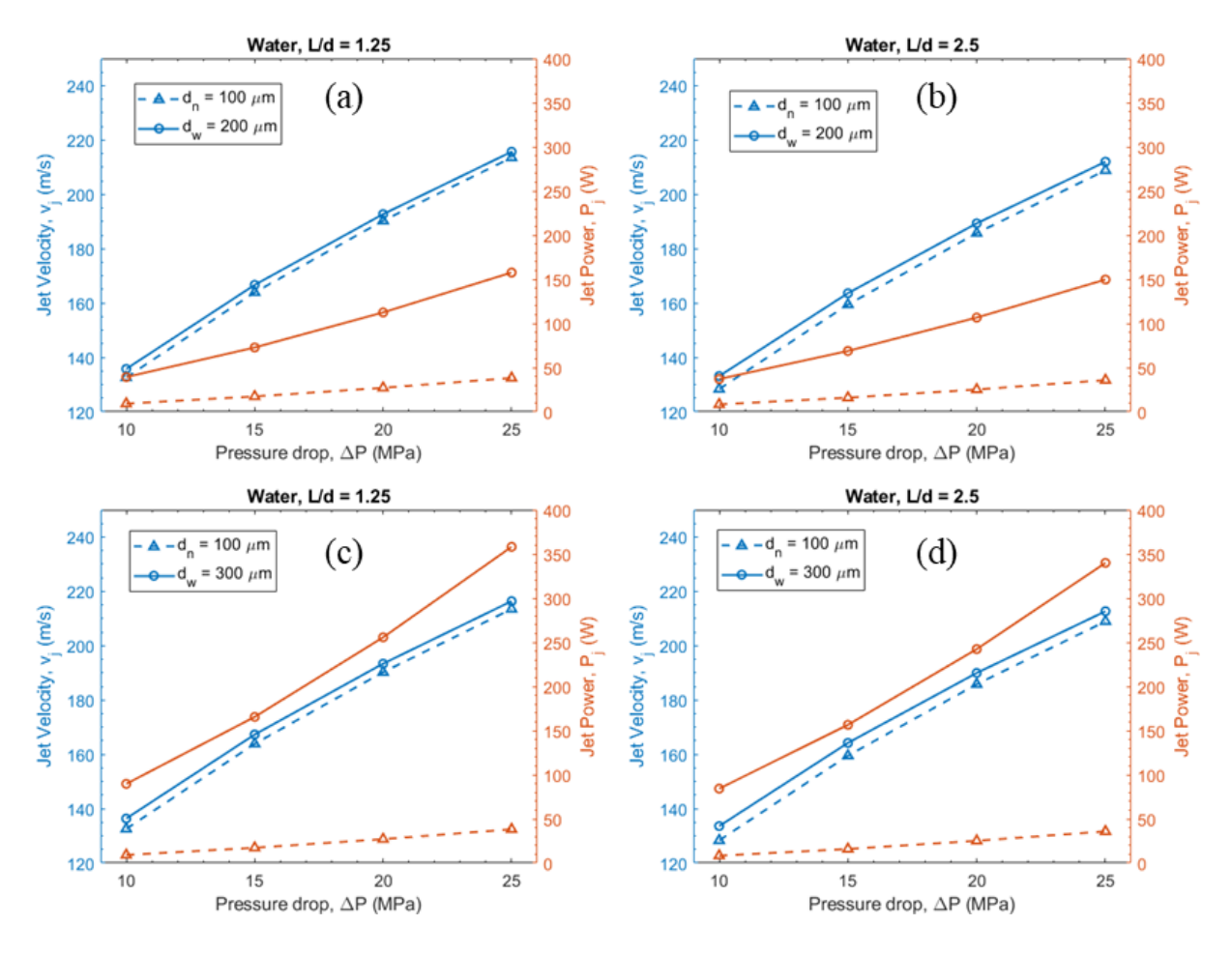


Figure 5. The effect of variation in upstream gauge pressure (ΔP) on jet velocity and power for water: (a) L/d = 1.25, $d_n = 100 \mu m$, $d_w = 200 \mu m$; (b) L/d = 2.5, $d_n = 100 \mu m$, $d_w = 200 \mu m$; (c) L/d = 1.25, $d_n = 100 \mu m$, $d_w = 300 \mu m$; (d) L/d = 2.5, $d_n = 100 \mu m$, $d_w = 300 \mu m$.

In figure 5(a), for the case of $d_n = 100 \, \mu m$ and $d_w = 200 \, \mu m$, an increase in pressure drop from 10 MPa to 25 MPa causes the jet velocity for the narrow orifice to increase (~61%) from 132.6 m/s to 213.5 m/s, and jet velocity for the wide orifice to increase (~58%) from 135.8 m/s to 215.7 m/s. As a result of this increase and the cubic dependence on jet speed (i.e., $P \propto v_j^3$), we observe an approximate 4-fold increase in jet power for both the narrow orifice (9.16 W \rightarrow 38.24 W) and wide orifice (39.31 W \rightarrow 157.6 W), both of which would result in deeper tissue penetration. Comparing figures 5(a) and 5(b), we observe that doubling the length of the orifice (straight section) has only a marginal effect, by reducing the jet velocities and powers, but the overall trends remain. For the larger wide orifices ($d_w = 300 \, \mu m$), shown in figures 5(c) and 5(d), the jet speeds for both the narrow and wide orifices are again very similar, with only ~1.3-3.7% variation. However, the increase in jet power for the wide orifice is more significant, with $P_w \approx 90 - 360$

W, due to the square-dependence on diameter, $P_j \propto d_j^2$. The observation that jet speeds are similar in all cases can be attributed to the fact that the orifice length (L/d = 1.25 – 2.5) does not permit the flow to fully develop, and flow in both orifices is turbulent at all driving pressures, with $Re_n \sim 1.3 \times 10^4 - 2.1 \times 10^4$ and $Re_w \sim 2.3 \times 10^4 - 6.4 \times 10^4$. Therefore, with the same pressure drop applied across both, we would expect similar jet speeds, notwithstanding the larger relative effect of the boundary layer for the narrow orifice, yielding a very slightly reduced speed compared to the wide orifice.

Given the near-linear variation in jet speed with pressure drop, it is also concluded that there is very little variation in the Euler number $Eu_n \sim 1.1 - 1.18$ and $Eu_w \sim 1.08 - 1.12$, indicating a similar mechanical efficiency in all cases. This observation was also reported in our earlier work⁴² using single-orifice geometries with a conical taper towards the orifice and is an artefact of the turbulent nature due to the low viscosity and high driving pressure.

For higher-viscosity fluids such as glycerin, previous studies ^{42,43,61,62} have indicated lower jet velocities as compared to low viscosity fluids like water, at the same driving pressure. This would naturally result in higher Euler numbers and lower Reynolds numbers, as detailed in Rane & Marston ^{42,43}. However, the increased role of friction for high-viscosity can also lead to significant heat generation ⁵⁹, which can in turn lower viscosity. Thus, the flow regimes for higher viscosity fluids are more caveated than those for low viscosity, and out-of-scope of the current work.

In effect, the Euler number is a proxy for mechanical efficiency by yielding the ratio of potential energy of the spring (upstream driving pressure) to kinetic energy of the jet (inertial pressure of the jet); since the upstream pressure required to produce a glycerin jet of ~200 m/s is significantly higher than that for water, the Euler number is higher and thus indicative of a less efficient system.

Since there is interdependence within the parameters used to characterize the performance of double-orifice jet injections (e.g., in jet power, $P \propto d_j^2 v_j^3$, but $v_j \sim d_j$), we thus use the *Eu-Re* parameter space as a concise way to elucidate the effects of orifice geometry and fluid viscosity on the hydrodynamic efficiency of the dual-orifice geometry, as shown below in figure 6:

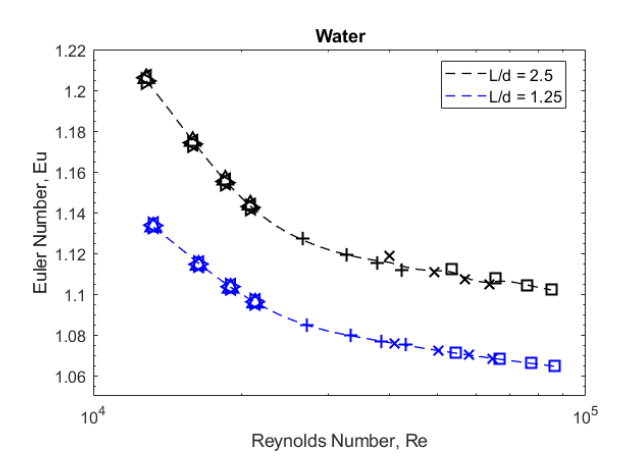


Figure 6. Euler number $((Eu)_n \text{ or } (Eu)_w)$ versus Reynolds number $((Re)_n \text{ or } (Re)_w)$. The dotted lines represent the smoothing spline fit to the data. The symbols correspond to orifice diameters as: $d_w = 400 \mu \text{m}$ (\Box), $d_w = 300 \mu \text{m}$ (\times), $d_w = 200 \mu \text{m}$ (+), $d_n = 100 \mu \text{m}$ (Δ , D, A).

In figure 6, regardless of the orifice diameters and orifice lengths, all data points collapse to a single characteristic curve in the Eu-Re space for a given L/d ratio ($L/d = L_n/d_n = L_w/d_w$). This signifies that, the orifice geometries for the multi-orifice jet injection can be characterized with the use of orifice L/d ratios.

For an intuitive understanding of figure 6, the inverse of Euler number can be thought of as the mechanical efficiency of the system, meaning that the system becomes more efficient as Euler number decreases at high Reynolds numbers, with the inviscid limit of Eu=1. At this theoretical limit, all upstream pressure energy provided to the system will convert entirely to kinetic energy of the liquid jet through the orifice. Indeed, we observe the asymptotic behavior as $Eu \rightarrow 1$ for water with $Re \rightarrow 10^5$, implying the geometry is highly efficient at these conditions. Furthermore, a simple comparison of the data series for L/d indicates that for a corresponding Re, a relatively wider orifice (L/d=1.25) has a lower Eu than a narrow orifice (L/d=2.5). These results have implications for the design of new injectors since a more efficient system would result in a lower-power requirement for the actuation mechanism, be it a spring or compressed gas or voice coil. We must caveat these results and analyses by noting that the simulations are run in the absence of moving parts, which in practice would include a sliding piston with a water-tight seal (e.g., O-ring) that induces friction and necessarily lowers the energy conversion efficiency.

Nonetheless, the results here, along with previous results^{42,43} imply that tailoring of the orifice geometry is essential to achieve a certain jet velocity and jet power through the orifice geometry, especially in laminar flow regime. We postulate that using the orifice geometry-specific *Eu-Re*

data in figure 6, for a desired jet velocity, manufacturers can either regulate the upstream pressure (or force from actuation source) for a given orifice geometry or vary the orifice geometries (L/d ratio) for a fixed upstream pressure.

As discussed earlier, jet injection through a narrow orifice is targeted for ID drug delivery, whilst jet injection through a wide orifice is targeted for IM drug delivery. For dual-orifice designs, it is essential to estimate and potentially regulate the flow through each orifice for delivering accurate dosage at desired penetration depths. Recent publications 49,50,63 provide information on the variation in jet penetration depth with respect to the variation in jet velocity for single-orifice jet injections. For example, with orifice diameter of 200 µm, McKeage et al.63 reported that an increase in jet velocity from 100 m/s to 140 m/s, corresponding to jet power increase from 15.7 W to 43.1 W, resulted in an increase of maximum jet penetration depth from ~ 5 mm to ~ 21 mm, for jet injection in porcine tissue. For our study herein, figure 5(a) provides jet powers in a similar range to those mentioned in McKeage et al. 63; for the narrow orifice (100 μ m), $P_i = 9.16$ W (at jet velocity of 132.6 m/s), and for the wide orifice (200 μ m), $P_i = 39.31$ W (at jet velocity of 135.77 m/s). For this case, in figure 7(a), the volumetric flow through wide orifice is approximately 4 x higher than the volumetric flow through narrow orifice. Meaning that, for a total cartridge volume of 1mL, ~ 0.2 mL will be delivered to shallow penetration depth (ID drug delivery) and ~ 0.8 mL will be delivered to deeper penetration depth (IM drug delivery). This is in accordance with the typical 20,22 drug dosage amounts used for IM drug delivery (0.5 ml – 2 ml), but slightly higher than that for ID drug delivery ($\sim 0.1 \text{ ml}$).

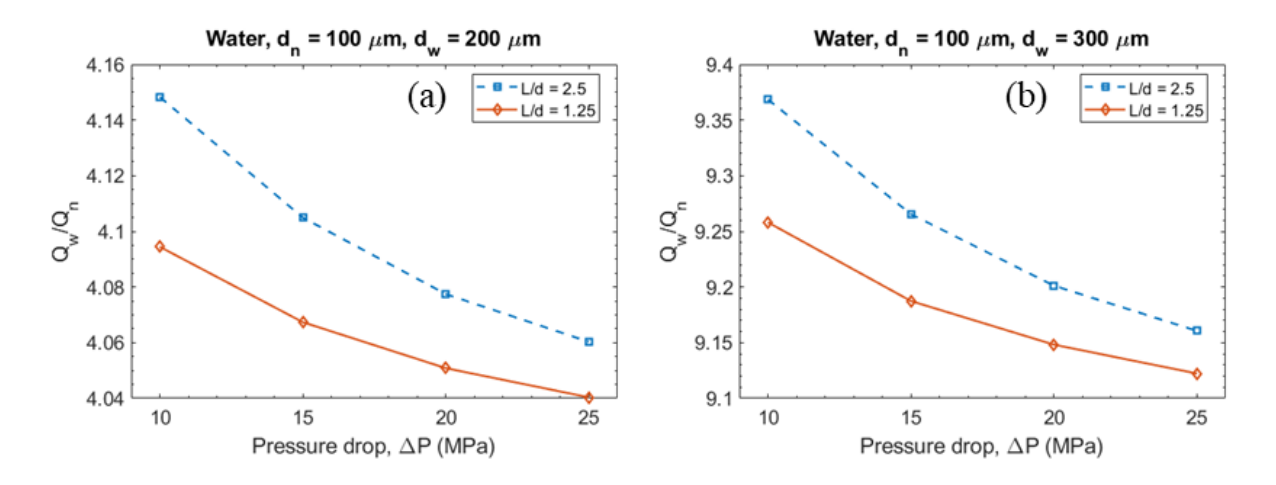


Figure 7. Effect of upstream gauge pressure (pressure drop) on the ratio of volumetric flow rates through wide and narrow orifices (Q_w/Q_n) . (a) Water, $d_n = 100\mu m$, $d_w = 200\mu m$; (b) Water, $d_n = 100\mu m$, $d_w = 300\mu m$.

Here, we perform a simple semi-dimensional analysis, to correlate the ratio of volumetric flow through the wide and narrow orifices: As expected, the volumetric flow rate through wide orifice (Q_w) is higher as compared to the volumetric flow rate through narrow orifice (Q_n) , and thus the ratio $Q_w/Q_n > 1$ (as shown in figure 7). This implies that the injection with deeper penetration (i.e., IM delivery with the wide orifice) would receive a higher drug volume than the injection with shallow penetration depth (i.e., ID delivery with the narrow orifice). For the water cases shown in figure 7 ($Re_n > 13000 \& Re_w > 26500$), the variation in delivery ratio (Q_w/Q_n) is very small (4.04) -4.15) for $d_w/d_n = 2$, and similarly it is 9.12-9.37 for $d_w/d_n = 3$, showing that near the inviscid limit, we simply have $Q_w/Q_n \propto (d_w/d_n)^2$, with the slight discrepancy being due to small viscous effects and pressure losses in the contraction region. Ignoring the small difference in ratio for the different pressure drops, we can calculate the volume delivered to both target tissues as a function of wide orifice size and orifice aspect ratio, L/d, as shown in figure 8. Here, we also include data for $d_w = 400 \mu m$, and we observe that the volume delivered via the narrow orifice (targeting ID delivery) is insensitive to the orifice aspect ratio, which is again a manifestation of the near-inviscid flow regime for water. Given that the typical target fractional dose is 100 µL, these results indicate that a wide orifice of 300 µm would represent the best choice for a split ID/IM injection, since $V_{ID} \approx 100 \,\mu\text{L}$ in that configuration.

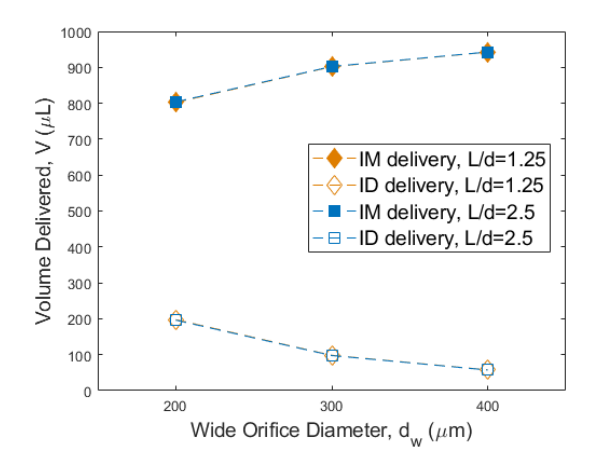


Figure 8. Volume delivered to either ID or IM tissues versus wide orifice diameter. In all cases, the narrow orifice is fixed at 100 µm. (a) Water - data points represent the average across the range of pressure drops due to the negligible differences.

This data once again illustrates that the effect of fluid viscosity notwithstanding, we can tailor the orifice diameter ratio and lengths to regulate flow rate (jet velocities) through narrow and wide orifices for the feasibility of simultaneous needle-free ID-IM drug delivery.

3.2. Preliminary in-vitro visualization

In the present study, we conducted preliminary experiments to investigate the feasibility of dual-orifice jet injection, using a modified Zetajet cartridge; the original orifice has a diameter of 113 μ m, which we use as the narrow orifice, whilst the wide orifice was created by using micro-drill bits with diameters of 300 and 400 μ m, respectively. In figure 9, snapshots of dyed water injection into gelatin are presented, which show dual jet streams emerging concurrently and depositing at different depths within the gelatin.

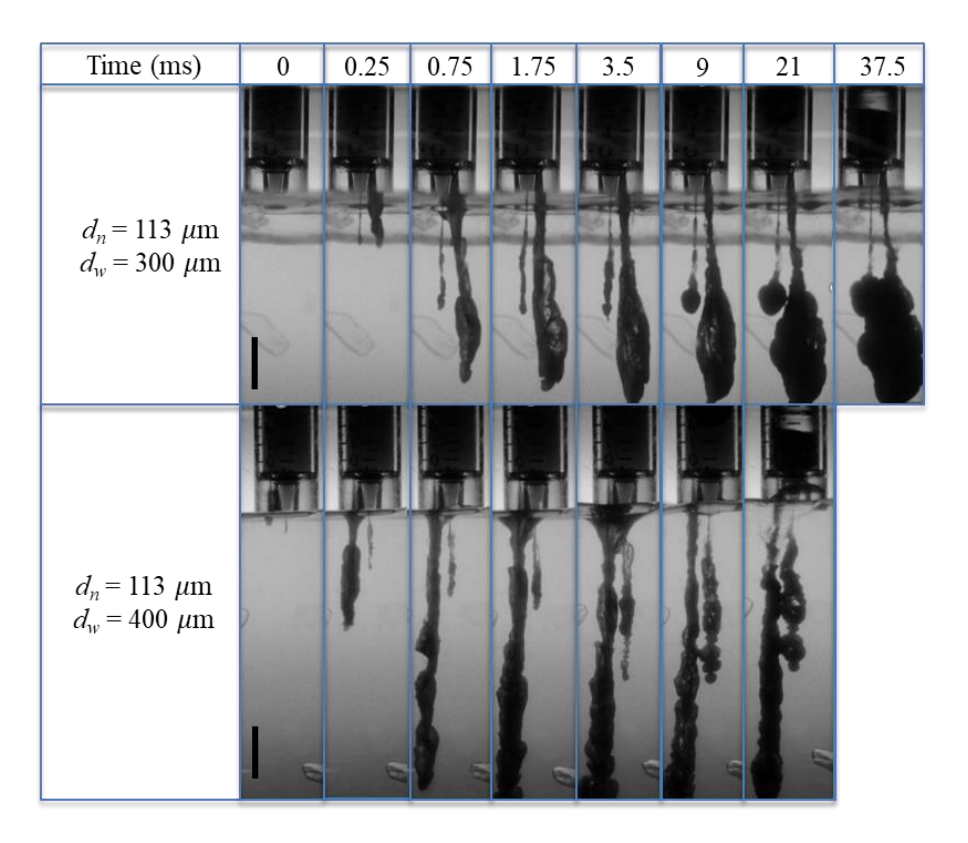


Figure 9. Dyed water injection into 5% gelatin hydrogel with a dual-orifice Zetajet cartridge. The cartridge outer diameter is 11.09mm, and the black scale bars in the first images are 10 mm long. Due to the increased flow rate through the 400 μ m wide orifice, the injection timeframe for the cartridge with 400 μ m wide orifice is only 21 ms, whereas the injection with cartridge having the wider orifice of 300 μ m extends to 37.5 ms.

In both cases presented in figure 9, the jet stream from the wide orifice has a significantly larger penetration depth as compared to the jet stream from the narrow orifice, and the stream from the 400 μ m orifice is also observed to penetrate deeper (~50 mm) than for 300 μ m (~33 mm), providing a direct illustration of the dependence of penetration depth on the jet velocity and diameter. Based on the data in figure 5, the approximate jet powers for these orifice diameters assuming ΔP ~15 MPa are ~165 W and ~17 W, respectively, thus showing these results are in

agreement with previous observations^{44,53} relating increased penetration depth to jet power. We note even the narrow jet stream punctures over 1 cm in these gelatin substrates, but the reader should keep in mind such homogenous tissue phantoms are poor proxies for true biological tissues where the discrete layers (ID/SC/IM) have vastly different properties.

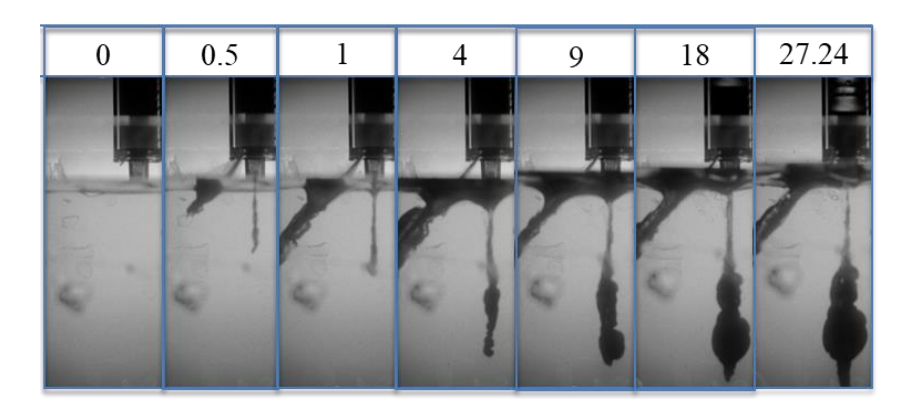




Figure 10. Dyed water injection into 59% gelatin hydrogel using a modified dual-orifice Zetajet cartridge. The wide orifice was drilled at an angle to modify injection depth. Angled wide orifice – 300 µm; Straight narrow orifice – 113 µm. Cartridge outer diameter is 11.09m. The color image to the right is the final view of the gelatin tank after injection.

Additionally, we experimented with a novel dual-orifice Zetajet cartridge whereby the wide orifice was drilled at an angle (~45°). The result of this configuration is shown in figure 10 for injection into gelatin. Whilst these images are descriptive of the potential of dual-orifice cartridges, we acknowledge that the experimental part of this work is at an early stage and that further experimental investigations with a more controlled manufacturing technique for creating dual orifices is necessary. At the time of writing, the authors are pursuing injection molding fabrication of novel designs with highly controlled orifice diameters.

3.3 Effect of viscous heat generation

In the work presented herein, we did not consider the effects of viscous heat generation, which occurs due to the high shear rate observed at the orifice. At the orifice, we can provide a first-order estimate of the average shear rate via $\dot{\gamma} \sim 2V_j/D_o$. Given jet speeds of $O(10^2)$ m/s and orifice diameters of $O(10^{-4})$ m, the average shear rate would be $\dot{\gamma} \sim O(10^6)$ s⁻¹, whilst near the boundary the shear rate could be an order of magnitude higher; in Rane & Marston $(2020)^{42,43}$ it was observed that the peak shear rate in the boundary layer reached up to 1.8×10^7 for water and 50% glycerol solutions, whilst in Williams et al. $(2019)^{59}$ it was reported to reach up to 2.7×10^8 for water and

 1.8×10^7 for 85% glycerol. At these high shear rates, the viscous friction results in a temperature increase that in turn can reduce the local viscosity of the fluid, thus providing a self-lubricating effect. Williams et al. (2019) provided the first report of this effect in the context of jet injectors, indicating that the local reduction in viscosity "assists" the jet formation process for high-viscosity fluids by increasing the jet speed than would otherwise be observed in the absence of this effect. In that work, it was assumed that the wall of the cartridge and orifice were adiabatic, thus restricting the heat to the fluid itself. Nonetheless, the observed temperature increase in the boundary layer for 85% glycerol was quite significant with $\Delta T \approx 30 - 40$ °C from the centerline to the wall, which the authors equated to a corresponding viscosity reduction from approximately 0.08 Pa.s at the center to 0.07 - 0.02 Pa.s in the boundary layer. As such, the heating creates a high-viscosity core (or plug) surrounded by low-viscosity annulus. Ultimately, the effect of this heating-induced viscosity reduction would be to lubricate the jet flow through the orifice and reduce the driving pressure required to sustain the flow for a desired jet speed. Whilst a full, comprehensive study of this effect is outside the scope of the present work, we present below snapshots of preliminary results (see fig. 11) from simulations that included temperaturedependent viscosity models. For simplicity, we focused these preliminary simulations on a single orifice with diameter of 150 μm, and fixed jet speeds of 75 m/s and 150 m/s, respectively. As such, these simulations utilized velocity inlet – pressure outlet boundary conditions for the purpose of highlighting the effect of the viscous heating. For these preliminary simulations, we ensured residual error for temperature and velocity components were at most 10⁻³ with a high density of (linear element order) mesh points (~630 /mm) in the nozzle exit region whereas a low density of mesh points ($\sim 22 \text{ /mm}$) was used in the upstream cartridge region.

In the example shown in figure 11, we observe that the high shear rate at the walls induces a maximum temperature increase of 86 K from the orifice centerline, with the most significant temperature rise ($\Delta T \approx 50$ K) occurring within ~10 µm of the walls. The corresponding viscosity reduction mirrors the temperature profile, with the core region ($r \le 40$ µm) exhibiting viscosity within 8% of the nominal value of 1.3 Pa.s, but a sharp reduction from approximately 0.95 to 0.61 Pa.s within ~10 µm of the walls. In Table 1 below, we have summarized the effects of viscous heating for two nominal jet speeds:

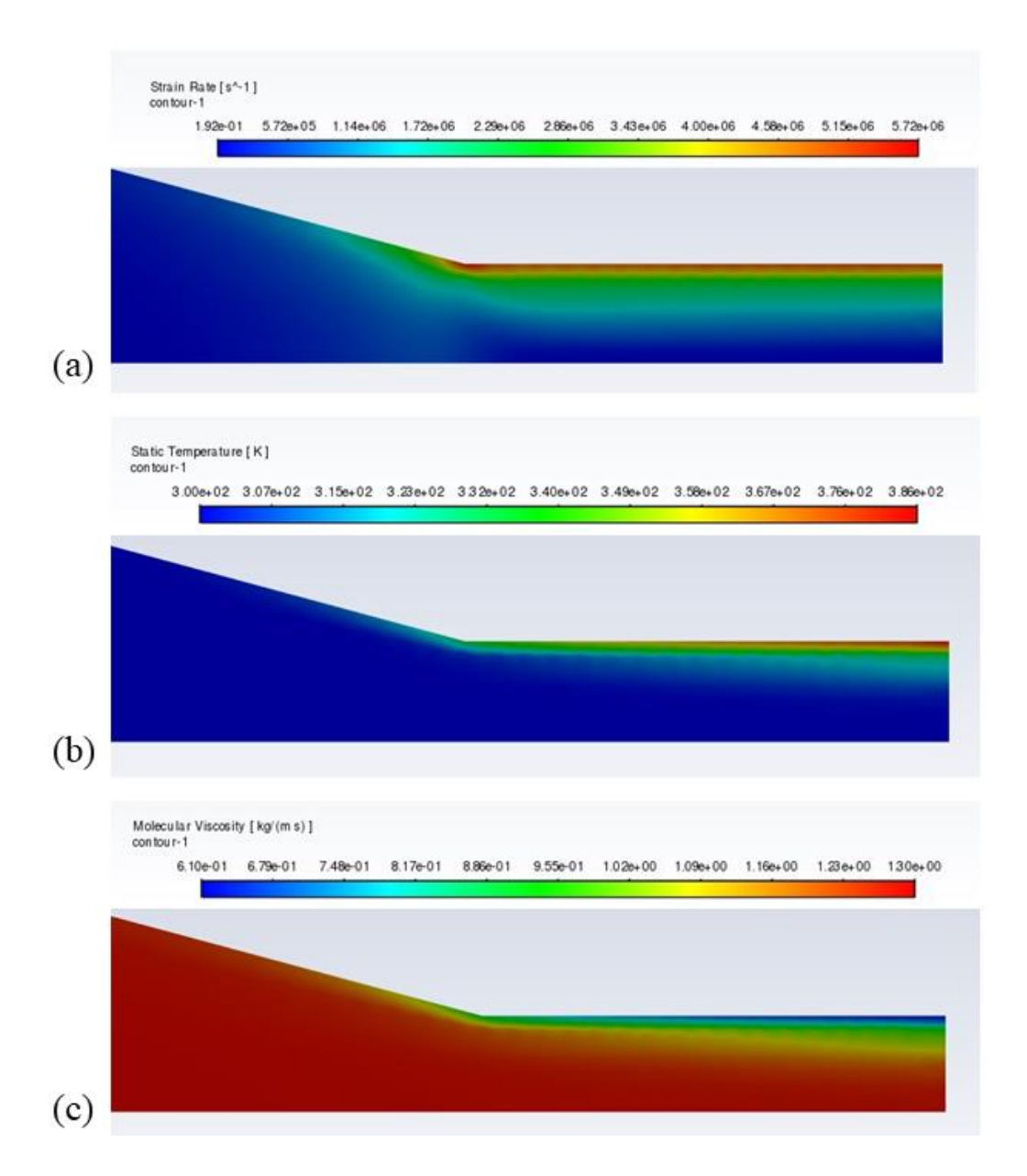


Figure 11. Snapshots near the orifice region from numerical simulations for flow of pure glycerine in a single orifice with D=150 μ m and average jet speed of $v_j=75$ m/s (max speed $v_{max}=134$ m/s) showing local fields for (a) Strain rate, (b) Temperature, and (c) Viscosity.

Fixed	Jet	Isothermal		With viscous heat generation		
Speed		(fluid inlet temp 300K)		(fluid inlet temp 300K, adiabatic walls)		
		Upstream driving	Viscosity	Upstream driving	Average	Average jet
		pressure (Pa)	(Pa.s)	pressure (Pa)	viscosity at	temperature
					orifice (Pa.s)	
75 m/s		7.15×10^{7}	1.30	5.65×10^{7}	1.02	327
150 m/s		1.61×10^{8}	1.30	1.1×10^{8}	0.9	346

Table 1. Summary of key data from numerical simulations for flow of pure glycerin in a single orifice with $D=150~\mu m$ and average jet speeds of $v_j=75~m/s$ and 150 m/s.

As evident from the values in Table 1, we observe that there is an increase in jet temperature (average temperature at the outlet), which causes a reduction in the average viscosity, which in turns causes a reduction in the driving pressure. This implies that the pressure required to sustain jet flow for high viscosity fluids is less than that calculated assuming isothermal conditions; in our two cases presented above, the reduction is approximately 20.9% for $v_j = 75$ m/s and 31.7% for $v_j = 150$ m/s. From a practical perspective, there are two implications of this finding; a lower driving pressure means that the mechanical components may experience less wear and improve lifetime of an injector device. Conversely, for a fixed force or driving pressure, it may be possible to achieve jet speeds with viscous fluids that are acceptable for injection purposes, i.e., the jet speed is high enough to provide jet dynamic pressures exceeding the critical stress of the skin, thus enabling puncture and effective drug delivery.

To caveat these preliminary findings, we must acknowledge that the simulations were conducted with adiabatic boundary conditions, and at steady-state. Whereas, in practice, the specific heat capacities of polycarbonate (a typical material used for injector cartridges) and glycerin are comparable (1.2 kJ/(kg.K) versus 2.43 kJ/(kg.K)), and the timescale of a typical injection (0.1 mL to 0.5 mL) is of the order of 0.03 to 0.6 seconds, and therefore highly transient in nature. As such, heat transfer at the walls and the transient nature of the jet injection process should be considered for a truly comprehensive treatment of the viscous heat generation. It is the intent of this preliminary section to spur further, comprehensive treatment of viscous heat generation in both experimental and computational studies.

4. Conclusions

In the literature, a combined intradermal (ID) and intramuscular (IM) drug delivery has been shown to elicit an enhanced, multi-faceted, and balanced immune response, especially for novel DNA vaccine delivery. Needle-based injection for combined ID – IM delivery may require multiple separate injections, which may not be preferable with regards to patient compliance and could result in extra sharps waste. In contrast, using a needle-free multi-orifice jet injection device, it is postulated that we could achieve simultaneous delivery to multiple penetration depths within a short timeframe (~10-100 ms).

In the present study, we considered a wide orifice (200 μ m – 400 μ m) for IM drug delivery and a narrow orifice (100 μ m) for ID drug delivery. Using numerical simulations, we studied the role of orifice diameter, and orifice length on jet power, jet velocity, and volumetric flow rate through each orifice. For low viscosity (water) it was found that driving pressures in the range 10-25 MPa lead to jet speeds ranging from approximately 140-230 m/s, which showed only a small dependence on the orifice diameter. Thus, the jet power, and hence the expected penetration depth, scaled primarily with diameter according to $P_j \propto d^2$. In terms of the volumetric flow ratio and volumes that could in theory be delivered to ID and IM tissues respectively, we found that diameters of 100 and 300 μ m for the narrow and wide orifices could result in approximately 100 μ l ID and 900 μ l IM for a full 1 ml injection, presenting acceptable volume deliveries to the respective target tissues.

By inspecting the results in the non-dimensional *Eu-Re* parameter space, it is clear that shorter orifices are preferred due to higher mechanical efficiency. The practical application of this result is that a more efficient system should preserve the lifetime of the fixed components of the injector (i.e., the main injector body and actuation mechanism).

Through some preliminary experiments, we visualized the penetration of wide and narrow jet streams into the gelatin substrates. The jet streams through the wide orifice showed significantly greater penetration depth as compared to the jet stream for the narrow orifice, due to increased jet power, as expected. Thus, we tentatively propose that it is indeed feasible to simultaneously deliver drugs to multiple penetration depths from the same injection cartridge using the needle-free jet injection technique with multiple orifices. Whilst continued efforts to improve the experimental techniques and visualization are ongoing, we hope that the work herein spurs new research into modified jet injection techniques. Other simple modifications to the cartridge geometry could include further refinement of the diameter ratios and placement of the orifices to further tailor the flow rate and hence jet speed in a given orifice. At the time of writing, a full, comprehensive treatment assessment of the viscous heating effects in a wide range of configurations (e.g., Newtonian vs non-Newtonian fluids, single vs multi-orifice, adiabatic vs heat-flux boundaries) in transient flow is underway.

Acknowledgement

We thank Inovio Pharmaceuticals for providing the Zetajet injection device and cartridges. This work was performed whilst YR was a PhD student at Texas Tech, with financial support from The National Science Foundation via award number CBET-1749382, awarded to JM. We would also like to thank the anonymous reviewers for providing excellent, thought-provoking critiques of the original work, which have greatly improved the manuscript.

References

- 1. Jagger, J., Hunt, E. H. & Pearson, R. D. Estimated Cost of Needlestick Injuries for Six Major Needled Devices. *Infect. Control Hosp. Epidemiol.* **11**, 584–588 (1990).
- 2. Kermode, M. Unsafe injections in low-income country health settings: Need for injection safety promotion to prevent the spread of blood-borne viruses. *Health Promot. Int.* **19**, 95–103 (2004).
- 3. Cook, I. F., Williamson, M. & Pond, D. Definition of needle length required for intramuscular deltoid injection in elderly adults: An ultrasonographic study. *Vaccine* **24**, 937–940 (2006).
- 4. Cook, I. F. Best vaccination practice and medically attended injection site events following deltoid intramuscular injection. *Hum. Vaccines Immunother.* **11**, 1184–1191 (2015).
- 5. Bancsi, A., Houle, S. K. D. & Grindrod, K. A. Shoulder injury related to vaccine administration and other injection site events. *Can. Fam. Physician* **65**, 40–42 (2019).
- 6. Gail B Cross, Jason Moghaddas, Jim Buttery, Sally Ayoub & Tony M Korman. Don't aim too high: Avoiding shoulder injury related to vaccine administration. *Aust. Fam. Physician* **45**, 303–306 (2016).
- 7. Soliman, E., Ranjan, S., Xu, T., Gee, C., Harker, A., Barrera, A. & Geddes, J. A narrative review of the success of intramuscular gluteal injections and its impact in psychiatry. *Bio-Des. & Manufacturing.* **1(3)**, 161–170 (2018).
- 8. White, S., Goodwin, J & Behan, L. Nurses' use of appropriate needle sizes when administering intramuscular injections. *J. Cont. Ed. Nursing* **49**, 519–526 (2018).
- 9. Mitragotri, S. Devices for overcoming biological barriers: The use of physical forces to disrupt the barriers. *Adv. Drug Deliv. Rev.* **65**, 100–103 (2013).
- 10. Prausnitz, M. R., Mitragotri, S. & Langer, R. Current status and future potential of transdermal drug delivery. *Nat. Rev. Drug Discov.* **3**, 115–124 (2004).
- 11. Mitragotri, S. Immunization without needles. *Nat. Rev. Immunol.* 5, 905–916 (2005).

- 12. Jayaprakash, V., Costalonga, M., Dhulipala, S. & Varanasi, K. K. Enhancing the Injectability of High Concentration Drug Formulations Using Core Annular Flows. *Adv. Healthc. Mater.* **9**, 1–7 (2020).
- 13. Guy, R. H. Current status and future prospects of transdermal drug delivery. *Pharmaceutical Research* vol. 13 1765–1769 (1996).
- 14. A. Charoo, N., Rahman, Z., A. Repka, M. & N. Murthy, S. Electroporation: An Avenue for Transdermal Drug Delivery. *Curr. Drug Deliv.* 7, 125–136 (2010).
- 15. Griffiths, U. K., Santos, A. C., Nundy, N., Jacoby, E. & Matthias, D. Incremental costs of introducing jet injection technology for delivery of routine childhood vaccinations: Comparative analysis from Brazil, India, and South Africa. *Vaccine* **29**, 969–975 (2011).
- 16. Aguiar, J. C. *et al.* Enhancement of the immune response in rabbits to a malaria DNA vaccine by immunization with a needle-free jet device. *Vaccine* **20**, 275–280 (2001).
- 17. Williams, J. *et al.* Hepatitis A vaccine administration: Comparison between jet-injector and needle injection. *Vaccine* **18**, 1939–1943 (2000).
- 18. Brocato, R. L. *et al.* Small animal jet injection technique results in enhanced immunogenicity of hantavirus DNA vaccines. *Vaccine* **39**, 1101–1110 (2021).
- 19. Sawamura, D. *et al.* In vivo gene introduction into keratinocytes using jet injection. *Gene Ther.* **6**, 1785–1787 (1999).
- 20. Jiang, J. *et al.* Integration of needle-free jet injection with advanced electroporation delivery enhances the magnitude, kinetics, and persistence of engineered DNA vaccine induced immune responses. *Vaccine* **37**, 3832–3839 (2019).
- 21. Haidari, G. *et al.* Combined skin and muscle vaccination differentially impact the quality of effector T cell functions: The CUTHIVAC-001 randomized trial. *Sci. Rep.* 7, 1–11 (2017).
- 22. Huang, G. *et al.* Combined radiofrequency ablation and ethanol injection with a multipronged needle for the treatment of medium and large hepatocellular carcinoma. *Eur. Radiol.* **24**, 1565–1571 (2014).
- 23. Cheeseman, H. M. *et al.* Combined Skin and Muscle DNA Priming Provides Enhanced Humoral Responses to a Human Immunodeficency Virus Type 1 Clade C Envelope Vaccine. *Hum. Gene Ther.* **29**, 1011–1028 (2018).
- 24. Blazevic, V. *et al.* Induction of human immunodeficiency virus type-1-specific immunity with a novel gene transport unit (GTU)-MultiHIV DNA vaccine. *AIDS Res. Hum. Retroviruses* **22**, 667–677 (2006).
- 25. Janeway, C., Travers, P., Walport, M. & Shlomchik, M. *Immunobiology*. (New York: Garland Science., 2001).
- 26. Combadiere, B. & Liard, C. Transcutaneous and intradermal vaccination. *Hum. Vaccin.* 7, 811–827 (2011).
- 27. Vasan, S. *et al.* In Vivo Electroporation Enhances the Immunogenicity of an HIV-1 DNA Vaccine Candidate in Healthy Volunteers. *PLoS One* **6**, e19252 (2011).

- 28. Rathore, N. *et al.* Characterization of protein rheology and delivery forces for combination products. *J. Pharm. Sci.* **101**, 4472–4480 (2012).
- 29. Burckbuchler, V. *et al.* Rheological and syringeability properties of highly concentrated human polyclonal immunoglobulin solutions. *Eur. J. Pharm. Biopharm.* **76**, 351–356 (2010).
- 30. Pstras, L. Valsalva manoeuvre using a syringe: Physics and implications. *Emergency Medicine Journal* vol. 33 831 (2016).
- 31. Mann, J. F. S. *et al.* Enhanced Immunogenicity of an HIV-1 DNA Vaccine Delivered with Electroporation via Combined Intramuscular and Intradermal Routes. *J. Virol.* **88**, 6959–6969 (2014).
- 32. Koutsonanos, D. G. *et al.* Delivery of subunit influenza vaccine to skin with microneedles improves immunogenicity and long-lived protection. *Sci. Rep.* **2**, 357–357 (2012).
- 33. Przybyla, B. *et al.* Aging alters macrophage properties in human skeletal muscle both at rest and in response to acute resistance exercise. *Exp. Gerontol.* **41**, 320–327 (2006).
- 34. Saclier, M., Cuvellier, S., Magnan, M., Mounier, R. & Chazaud, B. Monocyte/macrophage interactions with myogenic precursor cells during skeletal muscle regeneration. *FEBS Journal* vol. 280 4118–4130 (2013).
- 35. Kulkarni, V. *et al.* Comparison of intradermal and intramuscular delivery followed by in vivo electroporation of SIV Env DNA in macaques. *Hum. Vaccines Immunother.* **9**, 2081–2094 (2013).
- 36. Lin, F. *et al.* 327. A Novel Prototype Device for Electroporation-Enhanced DNA Vaccine Delivery to Both Skin and Muscle. *Mol. Ther.* **18**, S126 (2010).
- 37. Daellenbach, K.K.,End effector for needle-free Injection System, US Patent US2003/0163111 A1 (2003).
- 38. Crank, J.M., Devices, Systems, and related methods for delivery of fluid to tissue, US Patent US2015/0246178 A1 (2015)
- 39. Gilbert, S.J., Method for making a needle-free jet injection drug delivery device, US Patent US2007/0052139 A1 (2007).
- 40. Hunter, I.W., Taberner, A.T., Hemond, B.D., Wendell, D.W., Ball, N.B. & Hogan, N.C., Surface Injection Device, Europen Patent EP 1-848-480-B1 (2010).
- 41. McKeage, J.W., Tan, A.Z.H. & Taberner, A.J., Large volume subcutaneous delivery using multi-orifice jet injection, *Int. J. Pharm.*, **649**, 123605 (2023).
- 42. Rane, Y. S. & Marston, J. O. Computational study of fluid flow in tapered orifices for needle-free injectors. *J. Control. Release* **319**, 382–396 (2020).
- 43. Rane, Y. S. & Marston, J. O. Transient modelling of impact driven needle-free injectors. *Comp. Biol. Med.*, **135**, 104586 (2021).
- 44. Schramm-Baxter, J. & Mitragotri, S. Needle-free jet injections: Dependence of jet

- penetration and dispersion in the skin on jet power. J. Control. Release 97, 527–535 (2004).
- 45. Schramm-Baxter, J. R. & Mitragotri, S. Investigations of Needle-free Jet Injections. *26th Annu. Int. Conf. IEEE Eng. Med. Biol. Soc.* **4**, 3543–3546 (2004).
- 46. Chang, J. H., Hogan, C. N. & Hunter, I. W. High-speed X-ray imaging of needle-free jet injections. *Biomed. Imaging (ISBI)*, 2014 IEEE 11th Int. Symp. 473–476 (2014).
- 47. Baxter, J. & Mitragotri, S. Needle-free liquid jet injections: Mechanisms and applications. *Expert Rev. Med. Devices* **3**, 565–574 (2006).
- 48. Zeng, D. *et al.* A Mathematical Model and Experimental Verification of Optimal Nozzle Diameter in Needle-Free Injection. *J. Pharm. Sci.* **107**, 1086–1094 (2018).
- 49. Mohizin, A. & Kim, J-K., Conceptualization of a novel electromechanical system for small-volume needle-free jet injection, Eng. Appl. Comp. Fluid Mech., 17(1), 2240868 (2023)
- 50. Schoppink, J. & Fernandez-Rivas, D., Jet Injectors: Perspectives for small volume delivery with lasers, Adv. Drug Deliv. Rev., 182, 114109 (2022).
- 51. Baxter, J. & Mitragotri, S. Jet-induced skin puncture and its impact on needle-free jet injections: Experimental studies and a predictive model. *J. Control. Release* **106**, 361–373 (2005).
- 52. Zeng, D., Wu, N., Qian, L., Shi, H. & Kang, Y. Experimental investigation on penetration performance of larger volume needle-free injection device. *J. Mech. Sci. Technol.* **34**, 3897–3909 (2020).
- 53. Schramm, J. & Mitragotri, S. Transdermal drug delivery by jet injectors: Energetics of jet formation and penetration. *Pharm. Res.* **19**, 1673–1679 (2002).
- 54. Portaro, R., Sadek, J., Xu, H. & Ng, H. D. Controlled release using gas detonation in needle-free liquid jet injections for drug delivery. *Appl. Sci.* **9**, 2712 (2019).
- 55. Mohizin, A., Roy, K. E. R., Lee, D., Lee, S. K. & Kim, J. K. Computational fluid dynamics of impinging microjet for a needle-free skin scar treatment system. *Comput. Biol. Med.* **101**, 61–69 (2018).
- 56. Mohizin, A. & Kim, J. K. Effect of geometrical parameters on the fluid dynamics of airpowered needle-free jet injectors. *Comput. Biol. Med.* **118**, 103642 (2020).
- 57. Inoue, N. *et al.* Possibility and effectiveness of drug delivery to skin by needle-free injector. *Int. J. Pharm.* **391**, 65–72 (2010).
- 58. Wendell, D., Hemond, B., Hogan, N. C., Taberner, A. & Hunter, I. The Effect of Jet Parameters on Jet Injection. in *Proceedings of the 28th IEEE EMBS Annual International Conference* (2006). doi:10.1016/j.jconrel.2018.04.054.
- 59. Williams, R.M.J., McKeage, J.W., Ruddy, B.P., Nielsen, P.M.F. & Taberner, A.J., Viscous heating assists jet formation during needle-free jet injection of viscous drugs, *IEEE Trans. Biomed. Eng.*, **66(12)**, 3472-3479 (2019).
- 60. Rohilla, P., Lawal, I., Le Blanc, A., O'Brien, V., Weeks, C., Tran, W., Rane, Y.,

- Khusnatdinov, E. & Marston, J.O., Loading effects on the performance of needle-free jet injections in different skin models, *J. Drug Deliv. Sci & Tech.*, **60**, 102043 (2020).
- 61. Rane, Y. S., Thomas, J. B., Fisher, P., Broderick, K. E. & Marston, J. O. Feasibility of using negative pressure for jet injection applications. *J. Drug Deliv. Sci. Technol.* **63**, 102395 (2021).
- 62. Rohilla, P. *et al.* Characterization of jets for impulsively-started needle-free jet injectors: Influence of fluid properties. *J. Drug Deliv. Sci. Technol.* **53**, 101167 (2019).
- 63. McKeage, J.W., Ruddy, B.P., Nielsen, P.M.F & Taberner, A.J., The effect of jet speed on large volume jet injection, J. *Control. Rel.*, **280**, 51-57 (2018).